



Slip distribution from the 1 April 2007 Solomon Islands earthquake: A unique image of near-trench rupture

Ting Chen,^{1,2} Andrew V. Newman,¹ Lujia Feng,¹ and Hermann M. Fritz³

Received 5 June 2009; revised 7 July 2009; accepted 30 July 2009; published 27 August 2009.

[1] We estimate the slip distribution from the M_W 8.1 Solomon Islands earthquake in 2007, from two post-seismic surveys measuring uplifted coral and submerged coastal features. The occurrence of islands extremely proximal to the trench and nucleation of rupture allowed for the collection of unprecedented coseismic deformation dataset along a large megathrust earthquake. Using data from the two surveys along the southeastern half of the slip zone within five weeks of the event, we model the elastic dislocation to identify the optimal (29°), and alternate (20°), dip and distribution of thrust along the southern rupture. The vertical deformation, which includes both coseismic and early postseismic deformation, has highly variable and large slip within 25 km of the trench and straddling Ranongga Island. The shallow focus of slip in the near-trench area may explain the locally high tsunami run-up on portions of Simbo Island, however the aseismic contribution of afterslip remains unknown. **Citation:** Chen, T., A. V. Newman, L. Feng, and H. M. Fritz (2009), Slip distribution from the 1 April 2007 Solomon Islands earthquake: A unique image of near-trench rupture, *Geophys. Res. Lett.*, *36*, L16307, doi:10.1029/2009GL039496.

1. Introduction

[2] On April 1, 2007 a massive moment magnitude, M_W 8.1 earthquake ruptured the megathrust beneath the western Solomon Islands (Figure 1). The event caused a locally large tsunami striking more than 300 coastal communities in the Western and Choiseul Provinces resulting in 52 fatalities and significant damage to livelihood [McAdoo *et al.*, 2009]. Using coral uplift and subsidence data collected from two independent post-seismic surveys [Taylor *et al.*, 2008; Fritz and Kalligaris, 2008], we examine the spatial extent and variability of slip along the southeastern segment of the rupture zone, where subducted topography is diverse and significant local tsunami runup was measured. The tsunami runup peaked at 12 m on the northern tip of Simbo Island, washing away huts at Tapurai village (Figure 1) [Fritz and Kalligaris, 2008].

[3] The event ruptured the convergent plate interface along a portion of the southwestern Solomon Islands forming the San Cristobal Trench [e.g., Phinney *et al.*, 2004; Miura *et al.*, 2004; Taira *et al.*, 2004]. To the north, a

second subduction zone is consuming the Pacific plate and ~ 30 km thick Ontong Java Plateau [Miura *et al.*, 2004]. The subducting Pacific plate undercuts the thin active transform and ridge system to the south. Because of the unique dynamics of the subducted ridge, the earthquake ruptured across two subducting plates [Taylor *et al.*, 2008; Furlong *et al.*, 2009]. The earthquake initiated at the subduction interface of the downgoing Australian plate and ruptured westward across the downgoing Woodlark plate before terminating at the transition to the Solomon Sea plate where subduction of the Woodlark rise is ongoing (Figure 1). Here, the dual subduction is thought to change from a mode where the Pacific plate undercuts the Australian and Woodlark plates, to one in which Solomon Sea plate subduction dominates as Pacific subduction begins to strike more northward [e.g., Phinney *et al.*, 2004]. Subduction rates and directions change across the earthquake rupture zone from 96 mm a^{-1} of oblique convergence on the Australian plate to 106 mm a^{-1} of near-normal convergence on the Woodlark plate interface (rates compiled by Bird [2003]).

[4] The subduction of the active ridge creates a unique environment with diverse subducting plate physiography, generating a transect of exposed land immediately on either side of the trench. At the transition between the downgoing Woodlark and Australian plates, Simbo ridge forms Simbo Island immediately seaward of the trench. Only 7 km across the trench, Ranongga Island exists presumably from permanent deformation in the hanging wall due to the deflection of the subducted ridge. After the event, uplift and subsidence measurements made across this transect and other islands over the southeastern end of the rupture zone provide a unique data set to constrain combined coseismic and early afterslip along the shallow megathrust.

[5] An early reconnaissance between April 10th and 24th, 2007 covered more than 65 villages on 13 islands in the Western and Choiseul Provinces measuring 175 tsunami and runup heights [Fritz and Kalligaris, 2008], hereafter Fritz survey. Additionally, 37 measurements of rapid recent uplift and subsidence were recorded by the Fritz survey between April 12th and 20th, 2007 on 9 Islands (Figures 1b and 1c). Uplift was measured on exposed corals based on established methods [Taylor *et al.*, 1987; Briggs *et al.*, 2006; Meltzner *et al.*, 2006]. Subsidence was determined based on boat docks, submerged navigation obstacles and engulfed trees. A maximum uplift of 3.6 m was measured on southwestern Ranongga Island on April 12th, while a maximum subsidence of 1.5 m was observed on Simbo Island with an accuracy of ± 0.2 m correcting for predicted tides. A detailed land-level survey between April 16th and May 6th, 2007 measured co-seismic uplift and subsidence at 65 locations on 11 islands (Figures 1b and 1c) [Taylor *et al.*,

¹School of Earth and Atmospheric Sciences, Georgia Institute of Technology, Atlanta, Georgia, USA.

²School of Geodesy and Geomatics, Wuhan University, Wuhan, China.

³School of Civil and Environmental Engineering, Georgia Institute of Technology, Savannah, Georgia, USA.

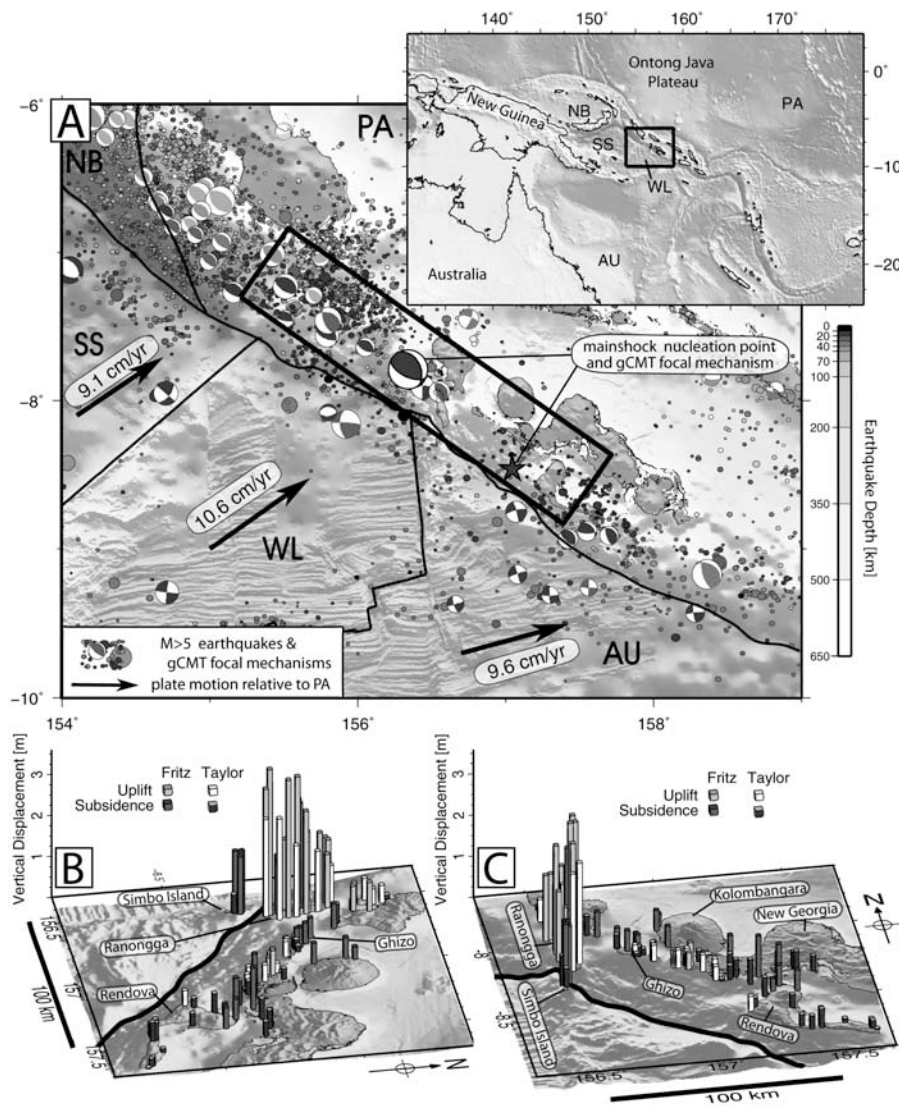


Figure 1. (a) Seismicity and regional plate motions of the study area. Shown are all recorded earthquakes (scaled by magnitude and shaded by depth) after 1962 for $M \geq 4$ (www.anss.org), and global centroid moment tensor (gCMT) focal mechanisms after 1976 for $M \geq 6$ [Ekström and Nettles, 1997]. Plate motions are shown for the Australian (AU), Woodlark (WL), Solomon Sea (SS), and North Bismarck (NB) microplates relative to stable Pacific plate (PA) (plate rates and boundaries are compiled by Bird [2003]). The approximate rupture area of the 1 April 2007, Solomon Islands M_W 8.1 earthquake, and model outline of this study (outlined rectangle), encompasses the point of rupture initiation (star) and slip-averaged gCMT solution. Inset shows study area (box) and the physiographic environment including the subducting Ontong Java Plateau to the north. (b and c) Shown are two views of the southeastern extent of the mainshock, where vertical deformation data were collected by two survey teams [Taylor et al., 2008; Fritz and Kalligaris, 2008].

2008], hereafter Taylor survey. Both survey teams visited key islands, however, differences exist in time and location of measurements. For example, the Taylor survey only measured displacements on the east side of Ranongga, with a maximum uplift of 2.46 ± 0.14 m (on May 6th), approximately 1.1 m less than that observed on the west side about 6 km away by the Fritz survey more than three weeks prior. The Taylor survey measurements are generally less extreme both in uplift and subsidence, ruling out systematic differences in datum as an explanation. Regional meteorological deviations from the predicted tides cannot be assessed due to the lack of local tide station data. Similar co-seismic

deformation patterns were determined based on satellite imagery [Taylor et al., 2008; Lubis and Isezaki, 2009].

2. Methods

[6] The uplifted coral reefs and other observed vertical changes in coastal features provide both coseismic and early post-seismic vertical motions. The geodetic data used contained only vertical deformation relative to the sea surface, thus we choose to model only the dip-slip component of motion along the megathrust. This choice is consistent with the global centroid focal mechanism (gCMT) solution [Ekström and Nettles, 1997] that suggests predom-

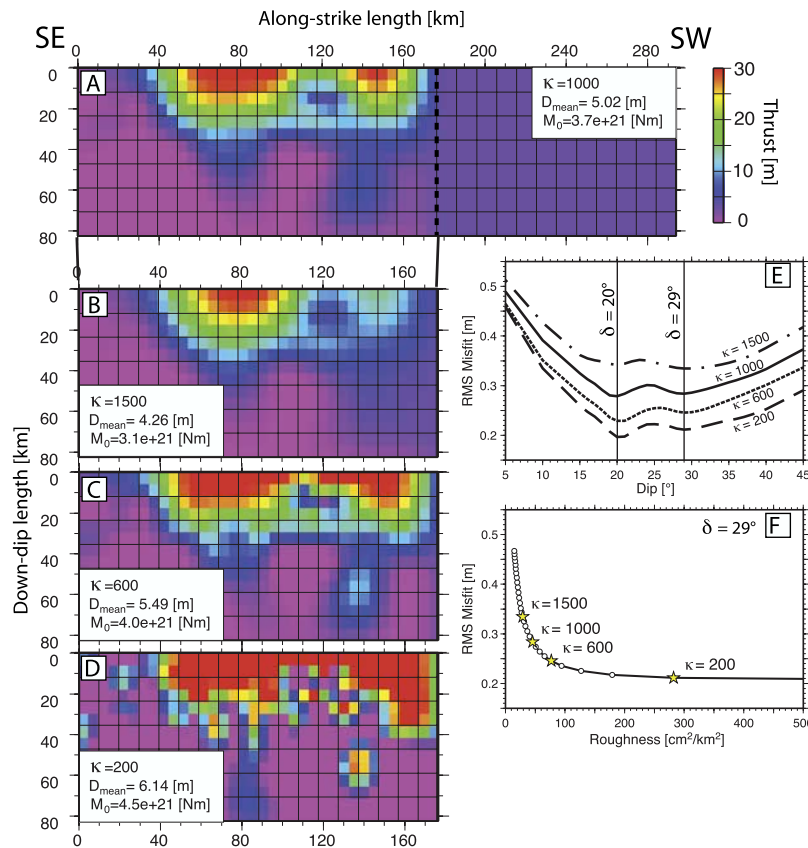


Figure 2. Models of distributed dip-slip along the subduction interface projected in Figure 1. Models are shown with the updip section at top and are projected with the southeast (SE) extent of the fault at 0 km along-strike and run to the southwest (SW) extent at 294 km. (a–d) As the smoothing parameter, κ increases, slip becomes more distributed and internal stress differentials are reduced. Our preferred model, Figure 2a at $\kappa = 1000$, was chosen by balancing the trade-off between misfit and smoothing. Thrust along the western 40% (along-strike position ≥ 176 km; dashed line in Figure 2a) is not resolvable by our models and is fixed at 3.0 m. (e) Lowest misfit solutions as a function of dip, δ show that 20 and 29° are minima over a range of smoothing. (f) The trade-off between solutions tested (open circles) for increased smoothing (decreased roughness) and increased misfit is shown for $\delta = 29^\circ$.

inantly thrust on a 37° north dipping plane. The uplift data density is sufficient in the eastern portion of the earthquake rupture zone to analyze the spatial variability in thrust there. We determine optimal solutions of dip-slip motion along discrete *Okada* [1992] dislocations defining the thrust plane. *Okada* [1992] dislocations describe a linear relationship between the modeled fault slip and predicted surface deformation, thus solutions for individual patches of slip can be superimposed as Green's functions that describe the total surface deformation field.

[7] For the Solomon Islands, we model the fault as striking 305°, the physiographic trend of the San Cristobal trench, and extending for northwest 294 km from Rendova Island (Figure 1; similar to the lengths described by *Taylor et al.* [2008] and *Furlong et al.*, [2009]). Because data only exists in the southeastern 60% of rupture, results are largely insensitive to the northwestern extent of the model. The optimal dip of the rupture interface is 29° and is further described below. Because the contribution of shallow rupture is important for estimating tsunami generation, we extend the model to the seafloor from a locking depth of 40 km, a reasonable maximum depth for interface rupture along a subduction zone [e.g., *Scholz*, 1998]. We discretize

the fault into a 60 by 14 grid of approximately 5 × 5 km uniform patches. While significant small and large-scale subducted topographic features are likely, particularly across the subducting Simbo Ridge, the interface morphology is not precisely known and hence we do not incorporate them in our model.

[8] To find the optimal slip distribution we used the Bounded Variable Least Squares method [e.g., *Stark and Parker*, 1995] to determine the optimal slip from individual patches within a finite range of possible solutions, solving for the l^2 -norm. We bound slip to a positive thrust less than 30 meters along the fault. The model resolution of fault slip for this event is highly variable, and is primarily controlled by the non-uniform spatial distribution of data, and depth of the modeled fault segment (see auxiliary material¹ for resolution testing). Deeper slip is reduced in magnitude and smoothed over a much larger region, while shallow slip is of large amplitude and highly localized. Because we lack coastal uplift data in the western ~40% of the fault, we constrain this region to 3 m of thrust (approximate mean slip for an $M_W = 8.1$ earthquake of comparable area and 30 GPa crustal rigidity). Testing a range of fixed thrust (between 2 and 8 m) in the unconstrained northwestern side had only

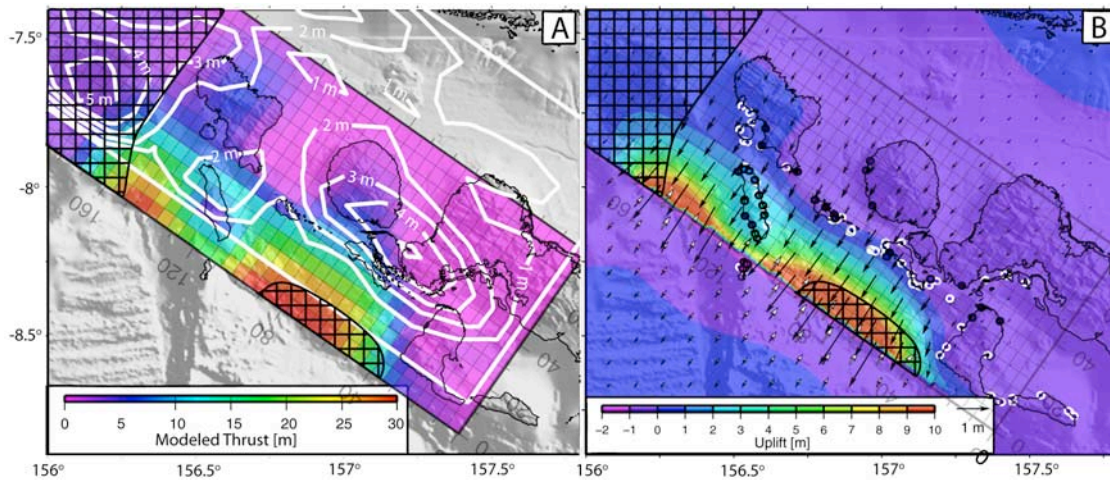


Figure 3. (a) Comparison between the optimal solution from this study (Figure 2a) and the fault model of *Furlong et al.* [2009]. Regions of low-to-no resolution (see Figures S2 and S3) in the geodetic model are covered by hatch marks. Slip is primarily in the shallow near-trench region, and largest on either side of Ranongga Island. Both models have two shallower and one deeper patch, however results from this study find deformation is generally shallower. (b) Modeled uplift, including the hinge-line of zero vertical deformation (dashed line) corresponds well to geodetic observations (circles: Fritz – black bordered; Taylor – white bordered). Arrows represent the predicted horizontal motion of the downgoing (white) and overriding plates (black). The region of maximum slip and modeled uplift is poorly resolved.

minimal effects on the slip distributions for the southeastern segment (<10% on adjacent patches), illustrating the limited resolution in the northwest.

[9] The lowest misfit solution is often one that considers the motion of discrete patches to be independent, causing highly variable slip distribution with slip defined primarily by patches immediately below an individual uplift measurement. However, because slip on one patch will enhance the activity of adjacent patches through rupture momentum, it is appropriate to constrain fault slip spatially across the model by incorporating a smoothing parameter. We follow the method described by *Harris and Segall* [1987] to incorporate the smoothing factor, κ that weights the second-order slip differential both along-strike and down-dip to reduce roughness (where $\kappa^2 = \beta$ by *Harris and Segall* [1987]). Introducing and increasing the smoothing parameter, however, comes at a cost of increased misfit between the predicted and observed deformation. Thus, finding an optimal solution with realistic slip, while maintaining low misfit is moderately subjective, and hence no single solution should be considered definitive.

[10] The dip, δ in this area is highly variable, increasing from near 0° to approximately 50° at 40 km depth [*Fisher et al.*, 2007]. Because the along-strike dip is unknown, and was identified as highly variable where observed, we found it was necessary to independently solve for a single dipping plane that describes the entire ruptured interface. To constrain the dip of the subduction interface we performed a series of inversions for faults ranging between 5° and 45° (Figure 2e). The solutions maintain a strong double-minima of root-mean-square (RMS) misfit over a range of κ at $\delta = 20^\circ$ and 29° that reflect a preferred value for each the Taylor and Fritz independent datasets, respectively. Our preferred solution of $\delta = 29^\circ$ is chosen because it is closer to the $\delta = 37^\circ$ – 38° found in the gCMT solution [*Ekström and Nettles*, 2007], and used by *Taylor et al.* [2008] for the uniform slip solution, however results at $\delta = 20^\circ$ (Figure S1 of the

auxiliary material) may better reflect the slip along the shallowest interface. An intermediate value of $\delta = 25^\circ \pm 5^\circ$ is found for the coseismic finite-fault model of *Furlong et al.* [2009].

3. Results and Discussion

[11] We explore the effects of increasing the smoothing parameter to determine the point at which further increases have the cost of markedly higher misfits for additional smoothing [e.g., *Jónsson et al.*, 2002]. At κ between 600 and 1200, we find reasonable trade-off between misfit and fault roughness, ρ , as defined by *Jónsson et al.* [2002] (Figure 2). At all tested smoothing values, slip in the shallow region continued toward the upper bound of the inversion model (30 m). The high slip values far exceed expected values for an M_w 8.1 event, and likely contain substantial afterslip. Resolution testing (Figures S2 and S3) suggest that the peak slip portion of the southeastern large slip patch is poorly resolved, and hence such high values should be disregarded (Figure 3). The northwestern patch just west of Ranongga Island is better resolved, yet the westward extend of shallow slip is undetermined by our models due to a lack of land for data. It is probable that a broader zone of more moderate slip, similar to that in the coseismic model of *Furlong et al.* [2009], is concentrated in a local high-slip patch here. Models testing the *Taylor et al.* [2008] and *Fritz and Kalligaris* [2008] surveys independently, similarly found two large shallow patches of displacement, but with reduced overall resolution (Figure S4). Though not resolvable by our modeling, the increased displacements from earlier Fritz survey may be the effects of short-term poroelastic deformation.

[12] The two large slip patches observed in our models are consistent with the coseismic finite-fault model derived from seismic body-wave modeling [*Furlong et al.*, 2009], but with geodetic slip predominantly occurring nearer the

trench (Figure 3). The models are inherently different in a number of ways: 1) this study incorporates up to one month of postseismic uplift, thus solutions are expected to be modestly larger than the coseismic only model; 2) Locally-derived geodetic solutions are mostly insensitive to rigidity, and hence better constrain the true slip in a region where rigidity may be poorly constrained; 3) The vertical-only data here only resolve the primarily thrust component of slip in this event, and only in the southeastern section where land coverage is significant; 4) Geodetic models have resolution that decreases proportionally with depth of the feature, hence small-scale slip features are geodetically best observed in the shallow trench; 5) The geographic location of the geodetic solution is locally referenced, while the seismic result is relative to a best estimate of the point of rupture nucleation [Furlong *et al.*, 2009; T. Lay, personal communication, 2009].

[13] Both of the preferred geodetic models of this study, and the finite-fault model of Furlong *et al.* [2009], are dominated by two updip patches, and one moderate patch downdip of the subducting Simbo ridge (Figure 3). The reduced shallow slip observed along the subducting ridge may be due to significant permanent deformation building Ranongga Island on the hanging wall, or from reduced interface coupling due to a thin and mechanically weak young ridge.

[14] The locations of the shallow slip patches are confirmed by the location of the hinge-line (0 uplift line) along the coast (Figure 3b), and consistent with the geodetic observations. The question whether most of this shallow slip occurred coseismically or as postseismic relaxation or afterslip, is not resolvable with the geodetic data alone. Tsunami data [Fritz and Kalligaris, 2008] and runup models using results from our study [Uslu *et al.*, 2008; Wei *et al.*, manuscript in preparation, 2009] yield mixed results. While our maximum modeled slip is likely overestimated, regionally large tsunami on Simbo's north tip and southwestern Ranongga with runup heights between 6 and 12 m, are of similar shape and magnitude, thus supporting coseismic generation of large slip along the western patch. This is further supported by the 5 m runup and tsunami damage on Choiseul Island located more than 100 km from the fault to the north of the New Georgia Sound, which are mostly likely reached by tsunami waves generated along the western patch [Fritz and Kalligaris, 2008]. However, the coastal areas on eastern Ranongga did not have significant tsunami damage, and hence any larger slip along the southeastern slip patch is likely postseismic. Significant shallow aseismic afterslip following the Solomon Island earthquake may be real. An interesting result of a GPS study following the $M_W = 8.7$ Nias Earthquake in 2005, was that considerable afterslip occurred mostly updip of the main event [Hsu *et al.*, 2006]. The shallow afterslip in the Nias earthquake, equivalent to a $M_W = 8.2$ earthquake, is comparable to the total shallow slip seen in the Solomon Islands event, an event with similar along-strike rupture.

4. Conclusions

[15] Using geodetic near-shore uplift and subsidence data in the southeastern 60% of the April 1st, 2007 – M_W 8.1 Solomon Islands earthquake, we identify highly variable,

predominantly shallow regions of slip about Ranongga island. Shallow slip is concentrated in two shallow patches updip of coseismic models derived from teleseismic body-waves. While the coseismic occurrence and absolute extent of thrust are not geodetically resolvable in these patches, tsunami runup data suggest the western patch was significantly coseismic.

[16] **Acknowledgments.** We thank the valuable discussions with T. Lay regarding the seismically resolved slip distribution of this event. We value the constructive and detailed reviews by two anonymous peers. Funded by Georgia Tech School of Earth and Atmospheric Sciences to AVN, Open Research Fund Program of Key Laboratory of Geomatics and Digital Technology (SD080704) and LOGEG to TC, NSF SGER-award CMMI-0646278 and UNESCO Intergovernmental Oceanographic Commission award IOC-4500034222 to HF.

References

- Bird, P. (2003), An updated digital model of plate boundaries, *Geochem. Geophys. Geosyst.*, 4(3), 1027, doi:10.1029/2001GC000252.
- Briggs, R. W., et al. (2006), Deformation and slip along the Sunda Megathrust in the great 2005 Nias-Simeulue earthquake, *Science*, 311, 1897–1901, doi:10.1126/science.1122602.
- Ekström, G., and M. Nettles (1997), Calibration of the HGLP seismograph network and centroid-moment tensor analysis of significant earthquakes of 1976, *Phys. Earth Planet. Inter.*, 101, 219–243, doi:10.1016/S0031-9201(97)00002-2.
- Fisher, M. A., E. L. Geist, R. Sliter, F. L. Wong, C. Reiss, and D. Mann (2007), Preliminary analysis of the earthquake (M_w 8.1) and tsunami of April 1, 2007, in the Solomon Islands, Southwestern Pacific Ocean, *Sci. Tsunami Hazards*, 26, 3–20.
- Fritz, H., and N. Kalligaris (2008), Ancestral heritage saves tribes during 1 April 2007 Solomon Islands tsunami, *Geophys. Res. Lett.*, 35, L01607, doi:10.1029/2007GL031654.
- Furlong, K., T. Lay, and C. Ammon (2009), A great earthquake rupture across a rapidly evolving three-plate boundary, *Science*, 324, 226–229, doi:10.1126/science.1167476.
- Harris, R., and P. Segall (1987), Detection of a locked zone at depth on the Parkfield, California, segment of the San Andreas fault, *J. Geophys. Res.*, 92, 7945–7962, doi:10.1029/JB092iB08p07945.
- Hsu, Y., M. Simons, J. Avouac, J. Galetzka, K. Sieh, M. Chlieh, D. Natawidjaja, L. Prawirodirdjo, and Y. Bock (2006), Frictional afterslip following the 2005 Nias-Simeulue earthquake, Sumatra, *Science*, 312(5782), 1921–1926, doi:10.1126/science.112696.
- Jónsson, S., H. Zebker, P. Segall, and F. Amelung (2002), Fault slip distribution of the 1999 M_W 7.1 Hector Mine earthquake, California, estimated from satellite radar and GPS measurements, *Bull. Seismol. Soc. Am.*, 92, 1377–1389, doi:10.1785/0120000922.
- Lubis, A. M., and N. Isezaki (2009), Shoreline changes and vertical displacement of the 2 April 2007 Solomon Islands earthquake M_w 8.1 revealed by ALOS PALSAR images, *Phys. Chem. Earth*, 34, 409–415, doi:10.1016/j.pce.2008.09.008.
- McAdoo, B. G., A. Moore, and J. Baumwoll (2009), Indigenous knowledge and the near field population response during the 2007 Solomon Islands tsunami, *Nat. Hazards*, 48, 73–82, doi:10.1007/s11069-008-9249-z.
- Meltzner, A. J., K. Sieh, M. Abrams, D. C. Agnew, K. W. Hudnut, J.-P. Avouac, and D. H. Natawidjaja (2006), Uplift and subsidence associated with the great Aceh-Andaman earthquake of 2004, *J. Geophys. Res.*, 111, B02407, doi:10.1029/2005JB003891.
- Miura, S., K. Suyehiro, M. Shinohara, N. Takahashi, E. Araki, and A. Taira (2004), Seismological structure and implications of collision between the Ontong Java Plateau and Solomon Island Arc from ocean bottom seismometer–airgun data, *Tectonophysics*, 389, 191–220, doi:10.1016/j.tecto.2003.09.029.
- Okada, Y. (1992), Internal deformation due to shear and tensile faults in a half-space, *Bull. Seismol. Soc. Am.*, 82, 1018–1040.
- Phinney, E. J., P. Mann, M. F. Coffin, and T. H. Shipley (2004), Sequence stratigraphy, structural style, and age of deformation of the Malaita accretionary prism (Solomon arc–Ontong Java Plateau convergent zone), *Tectonophysics*, 389, 221–224, doi:10.1016/j.tecto.2003.10.025.
- Scholz, C. H. (1998), Earthquakes and friction laws, *Nature*, 391, 37–42, doi:10.1038/34097.
- Stark, P. B., and R. L. Parker (1995), Bounded-variable least-squares: An algorithm and applications, *Comput. Stat.*, 10, 129–141.
- Taira, A., P. Mann, and R. Rahardiawan (2004), Incipient subduction of the Ontong Java Plateau along the North Solomon trench, *Tectonophysics*, 389, 247–266, doi:10.1016/j.tecto.2004.07.052.

- Taylor, F. W., C. Frohlich, J. Lecolle, and M. Strecker (1987), Analysis of partially emerged corals and reef terraces in the central Vanuatu arc: Comparison of contemporary coseismic and nonseismic with Quaternary vertical movements, *J. Geophys. Res.*, *92*, 4905–4933, doi:10.1029/JB092iB06p04905.
- Taylor, W., R. W. Briggs, C. Frohlich, A. Brown, M. Hornbach, A. K. Papabatu, A. J. Metzner, and D. Billy (2008), Rupture across arc segment and plate boundaries in the 1 April 2007 Solomons earthquake, *Nat. Geosci.*, *1*, 253–257, doi:10.1038/ngeo159.
- Uslu, B., Y. Wei, H. M. Fritz, V. Titov, and C. Chamberlin (2008), Solomon Islands 2007 tsunami near-field modeling and source earthquake deformation, *Eos Trans. AGU*, *89*(53), Fall Meet. Suppl., Abstract OS43D-1340.
-
- T. Chen, L. Feng, and A. V. Newman, School of Earth and Atmospheric Sciences, Georgia Institute of Technology, 311 Ferst Drive, Atlanta, GA 30332, USA. (anewman@gatech.edu)
- H. M. Fritz, School of Civil and Environmental Engineering, Georgia Institute of Technology, 210 Technology Circle, Savannah, GA 31407, USA.